science.sciencemag.org/content/366/6466/749/suppl/DC1

Supplementary Materials for

Efficient, stable solar cells by using inherent bandgap of α-phase formamidinium lead iodide

Hanul Min, Maengsuk Kim, Seung-Un Lee, Hyeonwoo Kim, Gwisu Kim, Keunsu Choi, Jun Hee Lee, Sang Il Seok*

*Corresponding author. Email: seoksi@unist.ac.kr

Published 8 November 2019, *Science* **366**, 749 (2019)
DOI: 10.1126/science.aay7044

This PDF file includes:

Materials and Methods

Synthesis

Formamidinium iodide (FAI) white powder was synthesized by reacting 20 mg of formamidine acetate salt (99%, Alfa Aesar) with 30 mL of hydroiodic acid (HI, 57 wt% in water, Aldrich) in a 250-mL round-bottom flask at 60℃ and 1-mbar pressure for 1 h with rotation. The products were dissolved in ethanol, recrystallized from diethyl ether, and finally dried at RT in a vacuum oven for 24 h. Formamidinium lead triiodide ($FAPbI_3$) powder was synthesized using synthesized FAI and lead iodide (99.99% PbI_2, TCI) mixture (1:1 molar ratio) in 11 mL of 2-methoxyethanol (anhydrous 99.8%, Aldrich) in a 70-mL vial with stirring. The mixed solution was heated up to 120℃ and then precipitated by retrograde method. Filtered $FAPbI_3$ black powder was baked at 150℃ for 30 min. Methlammonium lead tri-bromide ($MAPbBr_3$) powder, as an additive for fabricating the control $[(FAPbI_3)_{0.95}(MAPbI_3)_{0.05}]$ device, was synthesized using MABr and lead bromide (98% $PbBr_2$, Alfa) mixture in a 1:1 molar ratio in DMF by capturing single crystal with toluene. Here, methylammonium bromide (MABr) was synthesized by reacting methylamine solution (40 wt% in water, Aldrich) with hydrobromic acid (HBr, 48 wt% in water, Aldrich) (1:1.1 molar ratio) in a round bottomed flask at 0℃ for 3 hours under stirring. The product, was dissolved in ethanol, recrystallized from diethyl ether and dried at room temperature in a vacuum oven overnight.

Solar cell fabrication

Hole blocking layer titanium oxide (bl-TiO_2) was coated onto a fluorine doped tin oxide (FTO) glass (Asahi FTO glass, 12~13 Ω/cm^2) substrate by spray pyrolysis deposition of a 20 mM titanium diisopropoxide bis(acetylacetonate) (Aldrich) solution at 450 ℃. Mesoporous TiO_2 (mp-TiO_2) was spin-coated at 1500 r.p.m. for 40s on the blocking layer (bl)-TiO_2/FTO substrate

using a TiO_2 paste in 2-methoxyethanol (2ME) and terpinol (3.5:1 w/w). The films were calcined at 500℃ for an hour. Perovskite layers were spin-coated on mp-TiO_2/bl-TiO_2/FTO using the synthesized $FAPbI_3$ with x mol% methylenediammonium chloride ($MDACl_2$: x = 0, 1.9, 3.8, 5.7 mol%) or with 5 mol% of $MAPbBr_3$ (synthesized) in a mixed solvent of dimethylformamide (DMF) and dimethyl sulfoxide (DMSO) (8:1 v/v). The all perovskite precursor solution contained 35 mol% of methylammonium hydrochloride (MACl, 98% Aldrich). The all perovskite layer was first heat-treated at 150 ℃ for 10 minutes and annealed again at 100℃ for 10 minutes. For the surface passivation of perovskite film, octylammonium iodide, dodecylammonium iodide or phenethylammonium iodide (98%, Greatcell Solar) dissolved in isopropyl alcohol (IPA) (15 mM) was spin coated at 5000 rpm. The surface-treated film was dried at RT in a vacuum oven for 24 h or annealed at 100℃ for 5 min according to the passivation condition, and then spin-coated by hole transporting layer (HTL)/chlorobenzene (90 mg/1 mL) in a mixture of 39.5 μL of 4-tert-butylpyridine (TBP), 23 μL of Li-bis(trifluoromethanesulfonyl) imide (Li-TFSI)/acetonitrile (520mg/mL), and 10 μL of cobalt-TFSI dissolved in acetonitrile (375mg/mL) at 3000 r.p.m. for 30 seconds. Finally, a gold counter electrode was deposited by thermal evaporation (about 65-75 nm of thickness).

Characterization

J-V characteristics of the devices were measured using a Keithley 2420 source meter under illumination by a solar simulator (Newport, Oriel Sol3A class AAA) with an AM 1.5 filter and an irradiation intensity of 100 mW/cm^2. The active area was determined by the metal mask placed in front of the solar cell to avoid overestimation of the photocurrent density. Spectral mismatch factor of 1.05 was used for all J-V measurements. For the measurement of high-efficiency devices, an antireflective coating was applied to the surface. The stability test at continuous maximum power point (MPP) operation under 1 Sun, AM 1.5G illumination was

carried out in an ambient condition by fixing the voltage at V_{MPP} and then tracking the current output. The morphology of the films was measured using a scanning electron microscope (Cold FE-SEM, SU-8220). Space-charge-limited current (SCLC) characteristics of electron- and hole- only devices are measured by a Keithley 2636B. Grazing-incidence wide-angle x-ray scattering (GIWAXS) measurements were conducted at the PLS-II 6D UNIST-PAL beamline of Pohang Accelerator Laboratory. Nuclear magnetic resonance (NMR) analysis were measured by 400 MHz FT-NMR (Bruker, AVANCE III HD). IR measurements were conducted by Frontier FT-IR 6800 (Perkin Eimer). The crystal structure was analyzed using an X-ray diffractometer (D/MAX2500V/PC). X-ray photoelectron spectroscopy (XPS) analysis was measured by using Thermo Fisher Scientific (ESCALAB 250XI) equipment with Al Kα as the X-ray source. The optical properties of the films were measured using UV-Vis spectroscopy (Shimadzu UV-2600). Steady-state photoluminescence (PL) spectra were measured using a commercial time-correlated single photon counting (TCSPC) setup (FluoTime 300, PicoQuant GmbH) equipped with PMA-C-192-M detector, high-resolution excitation monochromators. The composition of the films was analyzed with secondary ion mass spectrometry (TOF-SIMS5, UNIST Central Research Facilities) with Bi^{3+} primary beam (25 keV, 1pA) and Cs^{+} sputter beam (1 KeV, 72 nA).

Computational method

We carried out the first-principles pseudopotential total energy calculations based on the density functional theory (DFT) within the generalized gradient density approximation (GGA) as implemented in the Vienna *ab initio* simulation package (VASP) (45-48). The electron-ion interactions are described employing the projector-augmented-wave (PAW) method (49) and Perdew-Burke-Ernzerhof (PBE) functional is used for GGA exchange correlation potential (50). To simulate stoichiometric and MDA- and Cl-doped $FAPbI_3$ in α-phase (33), we used a 3x3x3

supercell for all the calculations. A kinetic energy cutoff of 400 eV and only Γ k-point for Brillouin zone integration is employed. All the atomic positions and lattice parameters are fully relaxed until the total energy is converged within 10^{-4} eV.

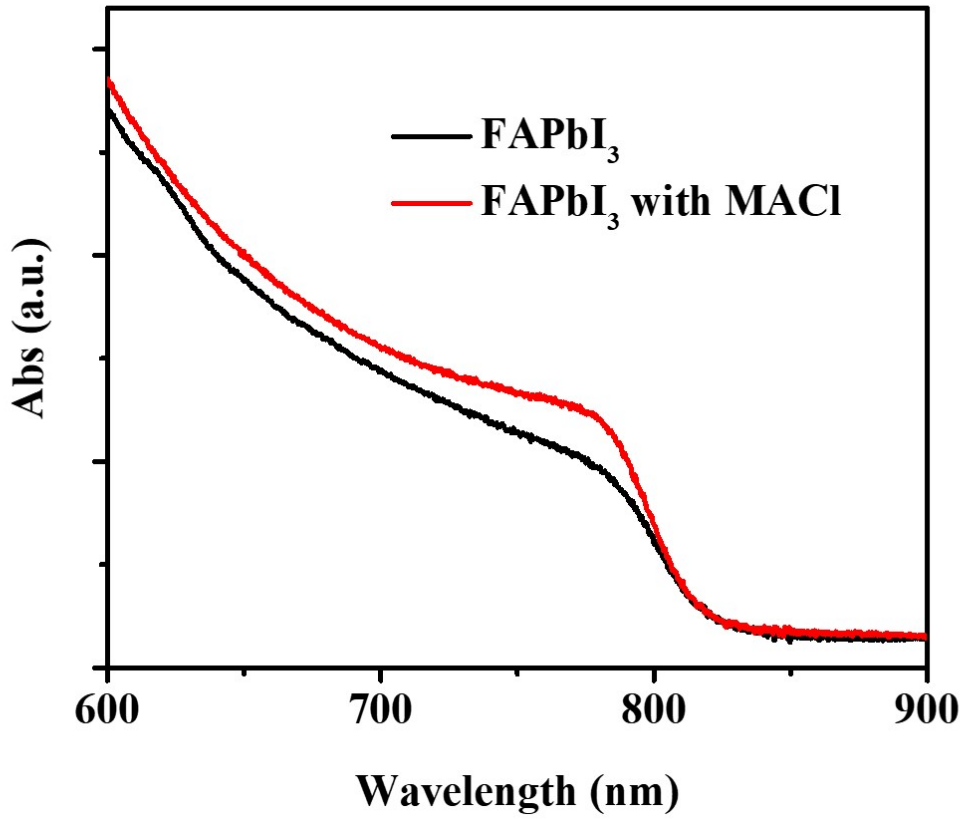

Fig. S1. Comparison of ultraviolet-visible (UV-vis) spectra of $FAPbI_3$ deposited with and without MACl additive.

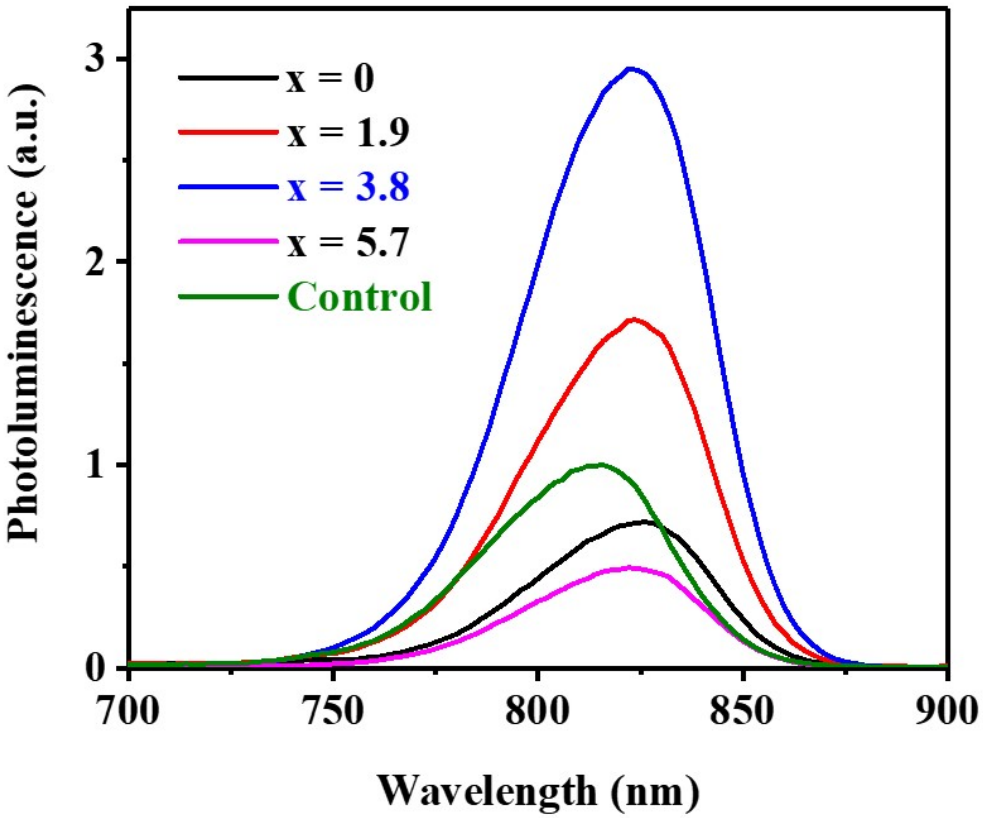

Fig. S2. Photoluminescence spectra for different x values of $FAPbI_3$:x$MDACl_2$ (x = 0, 1.9, 3.8, and 5.7 mol%) and control.

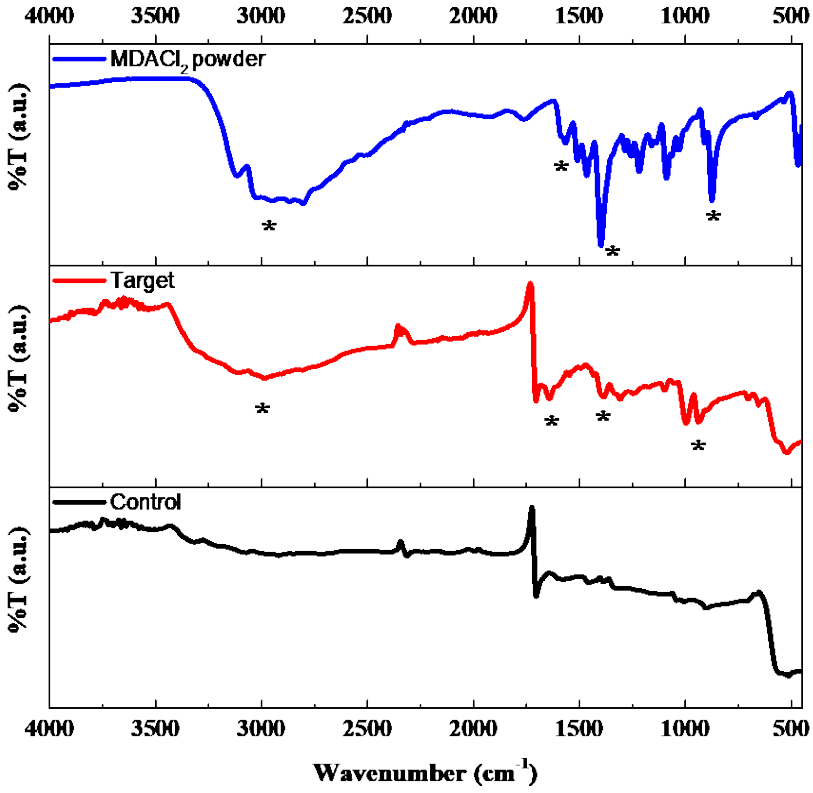

Fig. S3. Comparison of Fourier-transform infrared spectroscopy results of $MDACl_2$, target, and control.

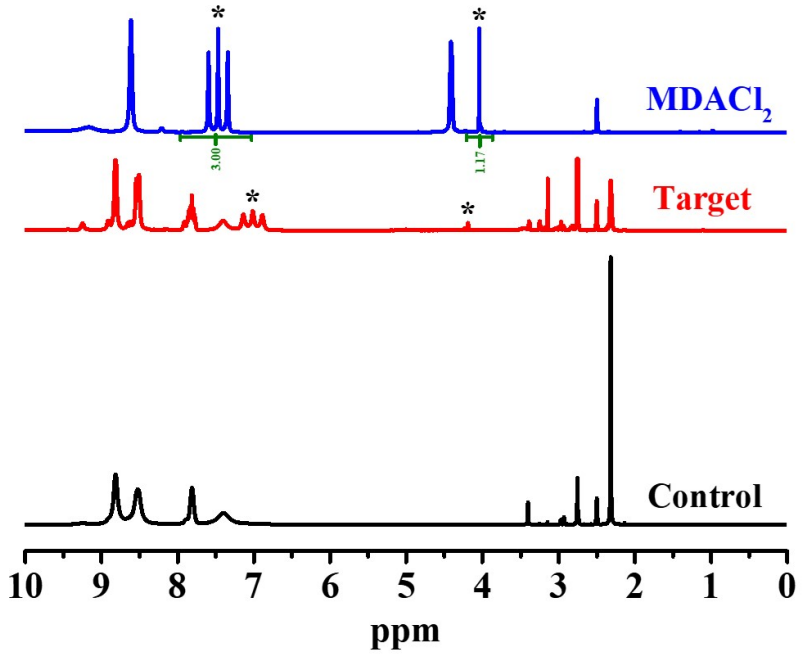

Fig. S4. Nuclear magnetic resonance (NMR) spectra of $MDACl_2$, target, and control.

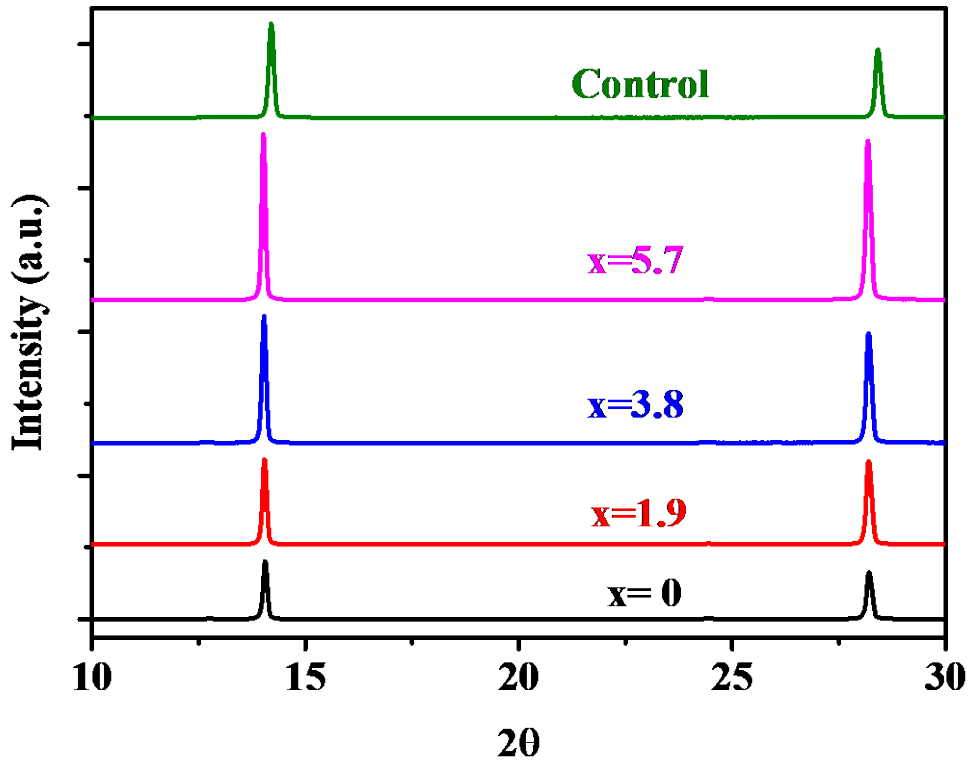

Fig. S5. X-ray diffraction (XRD) patterns of as-prepared $FAPbI_3$:x$MDACl_2$ (x = 0, 1.9, 3.8, and 5.7 mol%) and control.

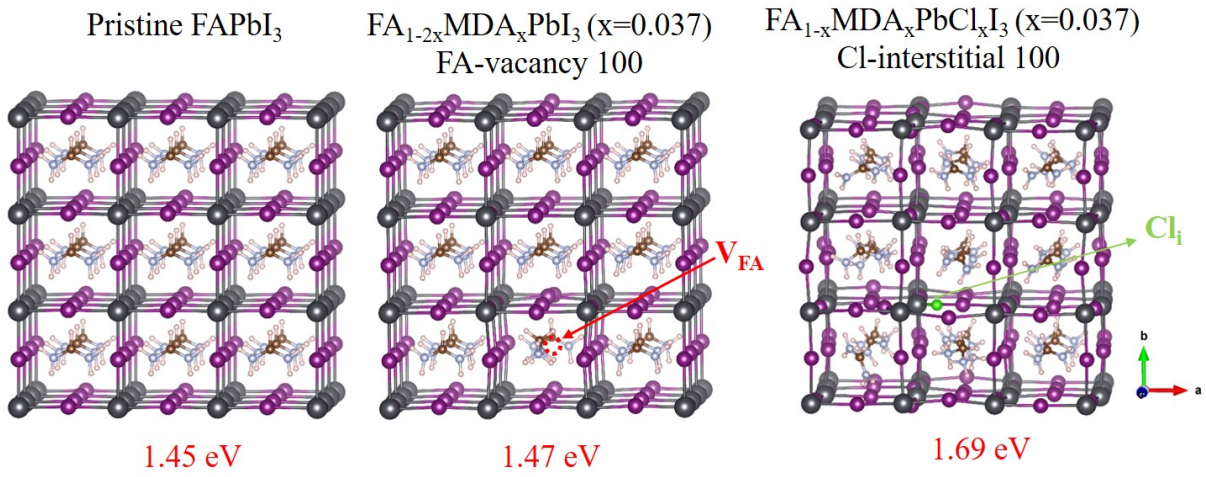

Fig. S6. Structure relaxation for the control Electronic band structures of $FAPbI_3$, $FA_{0.926}(V_{FA})_{0.037}MDA_{0.037}PbI_3$, and (c) $FA_{0.963}MDA_{0.037}PbI_3(Cl_i)_{0.037}$.

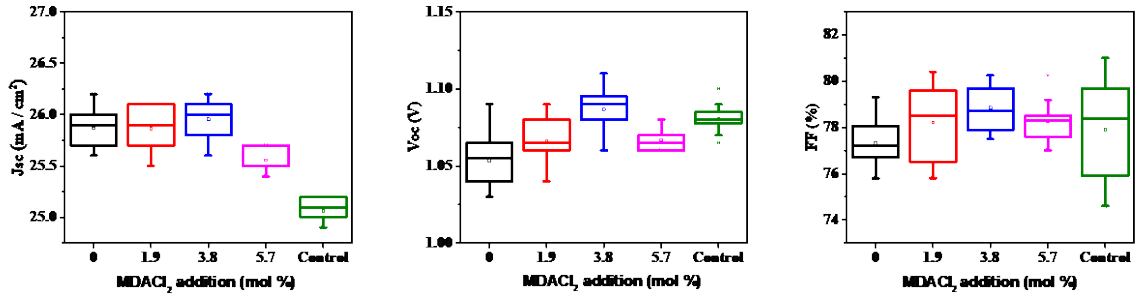

Fig. S7. Variation in J_{SC}, V_{OC}, and FF for different x values of $FAPbI_3$:x$MDACl_2$ (x = 0, 1.9, 3.8, and 5.7 mol%) and control.

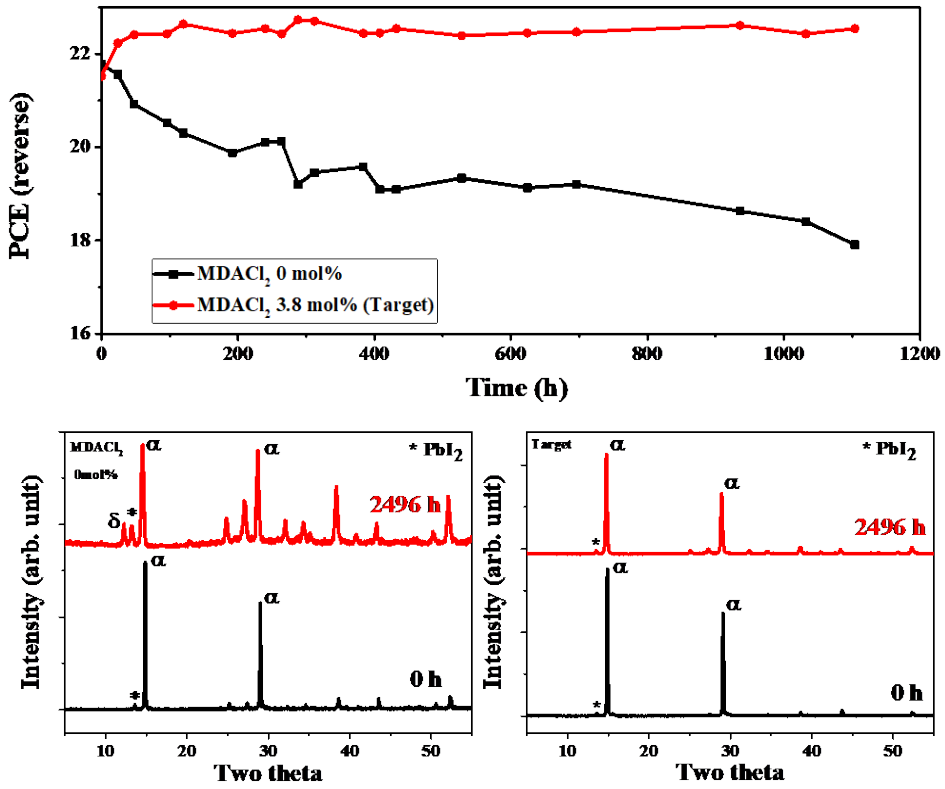

Fig. S8. Power conversion efficiency (PCE) change in FTO/bl-TiO_2/mp-TiO_2/Perovskite:$MDACl_2$ (0, 3.7 mol%)/Spiro-OMeTAD/Au (unencapsulated) measured over time stored under ambient conditions (RH 20-30%, 25 °C) in a dark and X-ray diffraction (XRD) patterns of resulting layers after 2500 h of operation time.

Table S1. Photovoltaic parameters of control and target, measured in reverse and forward mode, as extracted from Figure 2B.

	J_{sc} [mA/cm^2]	V_{oc} [V]	FF [%]	PCE [%]
Control_Rev	**25.14**	**1.14**	**80.55**	**23.05**
Control_For	**25.12**	**1.12**	**79.32**	**22.28**
Target_Rev	**26.50**	**1.14**	**81.77**	**24.66**
Target_For	**26.40**	**1.11**	**79.72**	**23.34**

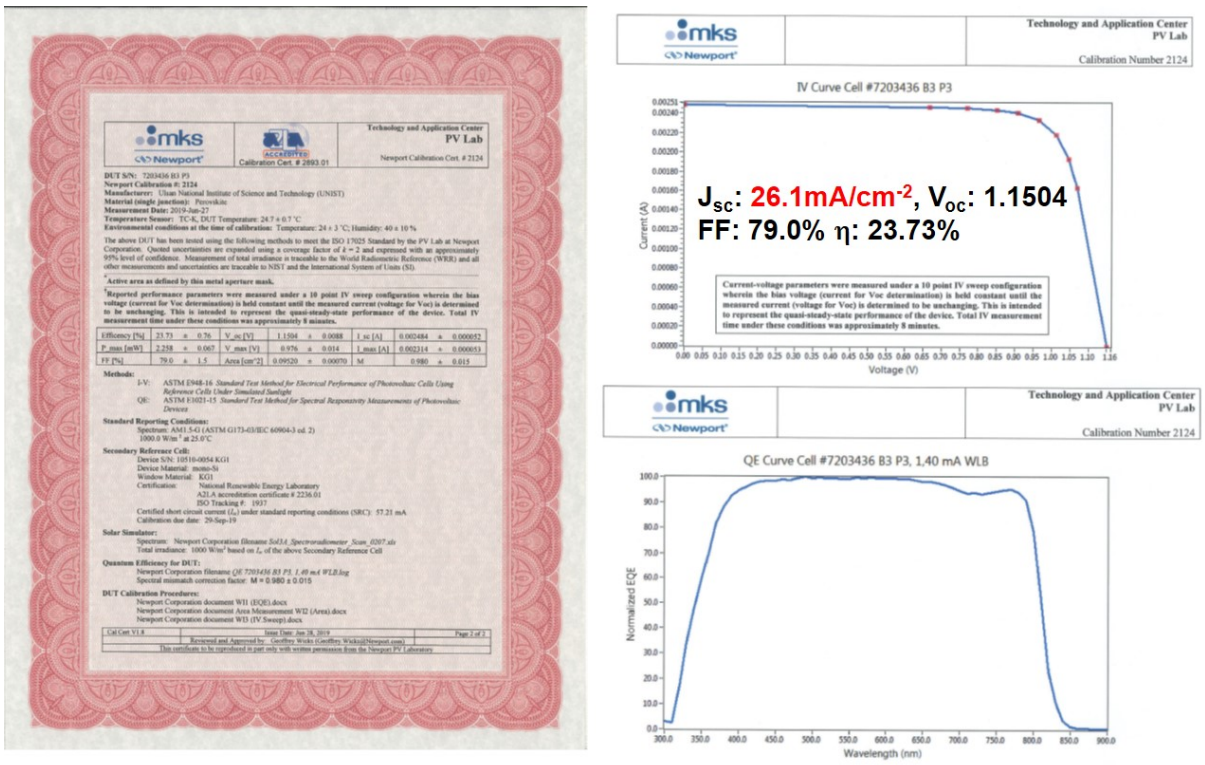

Fig. S9. Certified results from accredited photovoltaic certification laboratory (Newport, USA) for device shown in Figure 2B.

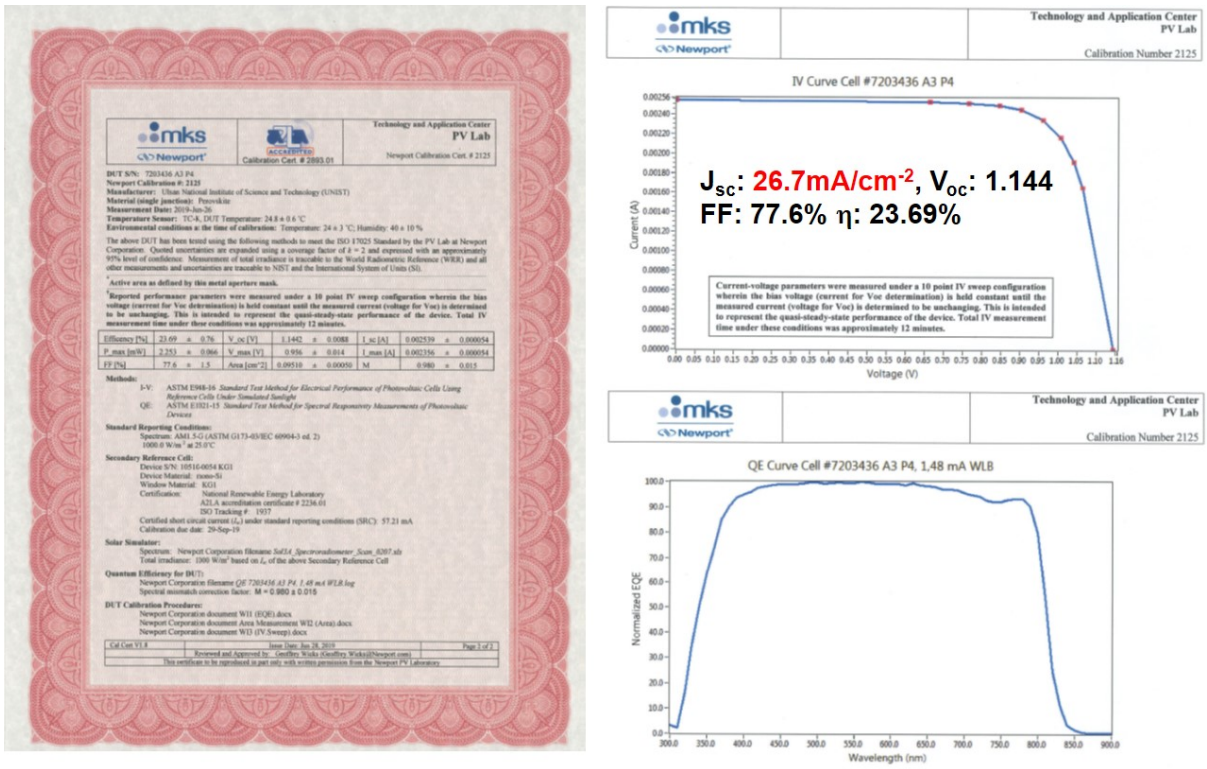

Fig. S10. Certified results from accredited photovoltaic certification laboratory (Newport, USA) for a second device.

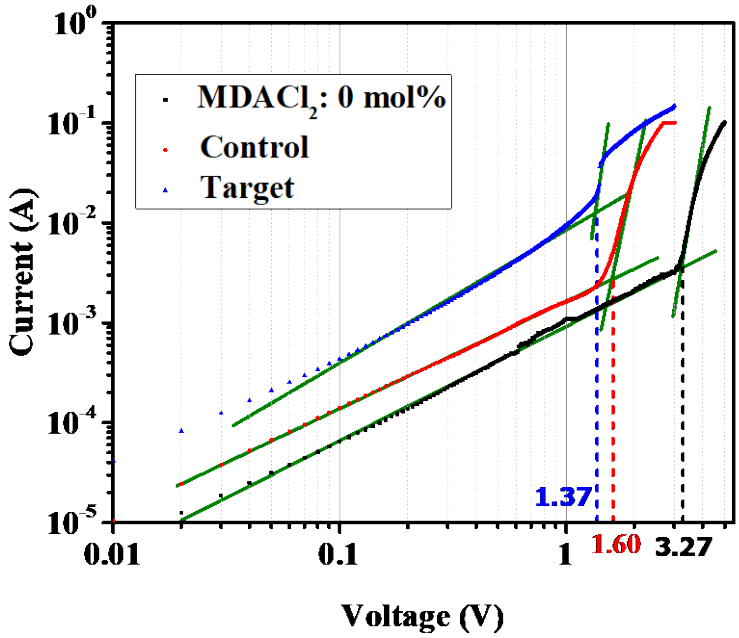

Fig. S11. Comparison of dark current–voltage curves of electron-only devices among representative control, target, and pure $FAPbI_3$ devices.

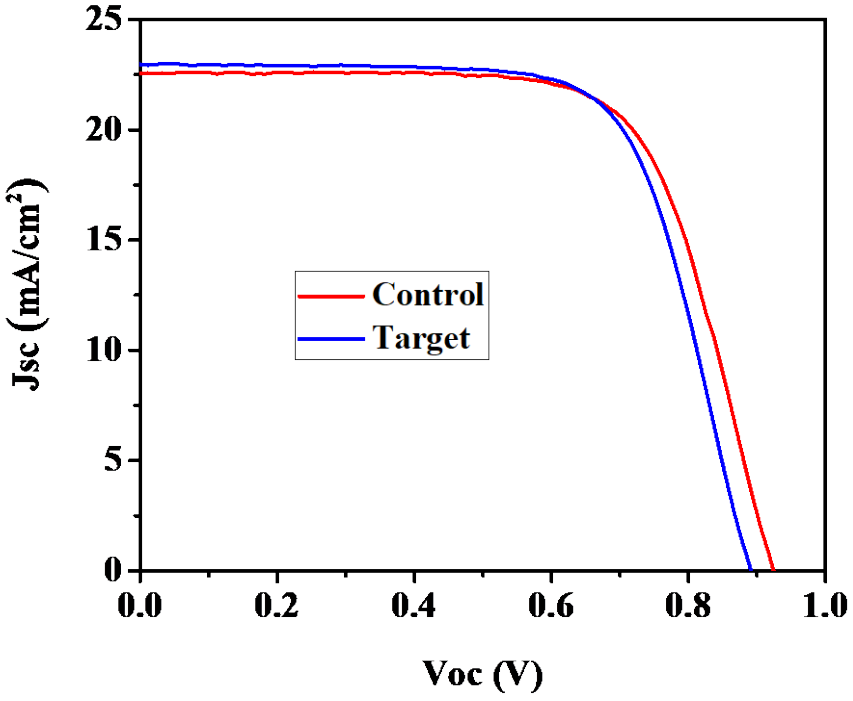

Fig. S12. J–V curves of control and target fabricated with CuPC as hole-transporting material instead of Spiro-OMeTAD.

Table S2. Photovoltaic parameters of control and target, fabricated with CuPC as hole-transporting material, as extracted from Figure S12.

As-fabricated	J_{sc} [mA/cm^2]	V_{oc} [V]	FF [%]	PCE [%]
Control	**22.57**	**0.926**	**69.02**	**14.44**
Target	**22.97**	**0.886**	**69.89**	**14.23**

References and Notes

1. Q. Han, S.-H. Bae, P. Sun, Y.-T. Hsieh, Y. M. Yang, Y. S. Rim, H. Zhao, Q. Chen, W. Shi, G. Li, Y. Yang, Single Crystal Formamidinium Lead Iodide (FAPbI3): Insight into the Structural, Optical, and Electrical Properties. *Adv. Mater.* **28**, 2253–2258 (2016). doi:10.1002/adma.201505002 Medline

2. G. E. Eperon, S. D. Stranks, C. Menelaou, M. B. Johnston, L. M. Herz, H. J. Snaith, Formamidinium lead trihalide: A broadly tunable perovskite for efficient planar heterojunction solar cells. *Energy Environ. Sci.* **7**, 982–988 (2014). doi:10.1039/c3ee43822h

3. A. Amat, E. Mosconi, E. Ronca, C. Quarti, P. Umari, M. K. Nazeeruddin, M. Grätzel, F. De Angelis, Cation-induced band-gap tuning in organohalide perovskites: Interplay of spin-orbit coupling and octahedra tilting. *Nano Lett.* **14**, 3608–3616 (2014). doi:10.1021/nl5012992 Medline

4. E. Smecca, Y. Numata, I. Deretzis, G. Pellegrino, S. Boninelli, T. Miyasaka, A. La Magna, A. Alberti, Stability of solution-processed MAPbI3 and FAPbI3 layers. *Phys. Chem. Chem. Phys.* **18**, 13413–13422 (2016). doi:10.1039/C6CP00721J Medline

5. T. M. Koh, K. Fu, Y. Fang, S. Chen, T. C. Sum, N. Mathews, S. G. Mhaisalkar, P. P. Boix, T. Baikie, Formamidinium-Containing Metal-Halide: An Alternative Material for Near-IR Absorption Perovskite Solar Cells. *J. Phys. Chem. C* **118**, 16458–16462 (2014). doi:10.1021/jp411112k

6. N. J. Jeon, J. H. Noh, W. S. Yang, Y. C. Kim, S. Ryu, J. Seo, S. I. Seok, Compositional engineering of perovskite materials for high-performance solar cells. *Nature* **517**, 476–480 (2015). doi:10.1038/nature14133 Medline

7. D. P. McMeekin, G. Sadoughi, W. Rehman, G. E. Eperon, M. Saliba, M. T. Hörantner, A. Haghighirad, N. Sakai, L. Korte, B. Rech, M. B. Johnston, L. M. Herz, H. J. Snaith, A mixed-cation lead mixed-halide perovskite absorber for tandem solar cells. *Science* **351**, 151–155 (2016). doi:10.1126/science.aad5845 Medline

8. M. Saliba, T. Matsui, J.-Y. Seo, K. Domanski, J.-P. Correa-Baena, M. K. Nazeeruddin, S. M. Zakeeruddin, W. Tress, A. Abate, A. Hagfeldt, M. Grätzel, Cesium-containing triple cation perovskite solar cells: Improved stability, reproducibility and high efficiency. *Energy Environ. Sci.* **9**, 1989–1997 (2016). doi:10.1039/C5EE03874J Medline

9. E. H. Jung, N. J. Jeon, E. Y. Park, C. S. Moon, T. J. Shin, T.-Y. Yang, J. H. Noh, J. Seo, Efficient, stable and scalable perovskite solar cells using poly(3-hexylthiophene). *Nature* **567**, 511–515 (2019). doi:10.1038/s41586-019-1036-3 Medline

10. N. J. Jeon, H. Na, E. H. Jung, T.-Y. Yang, Y. G. Lee, G. Kim, H.-W. Shin, S. Il Seok, J. Lee, J. Seo, A fluorene-terminated hole-transporting material for highly efficient and stable perovskite solar cells. *Nat. Energy* **3**, 682–689 (2018). doi:10.1038/s41560-018-0200-6

11. Q. Jiang, Y. Zhao, X. Zhang, X. Yang, Y. Chen, Z. Chu, Q. Ye, X. Li, Z. Yin, J. You, Surface passivation of perovskite film for efficient solar cells. *Nat. Photonics* **13**, 460–466 (2019). doi:10.1038/s41566-019-0398-2

12. E. T. Hoke, D. J. Slotcavage, E. R. Dohner, A. R. Bowring, H. I. Karunadasa, M. D. McGehee, Reversible photo-induced trap formation in mixed-halide hybrid perovskites for photovoltaics. *Chem. Sci.* **6**, 613–617 (2015). doi:10.1039/C4SC03141E Medline

13. J.-W. Lee, Z. Dai, T.-H. Han, C. Choi, S.-Y. Chang, S.-J. Lee, N. De Marco, H. Zhao, P. Sun, Y. Huang, Y. Yang, 2D perovskite stabilized phase-pure formamidinium perovskite solar cells. *Nat. Commun.* **9**, 3021 (2018). doi:10.1038/s41467-018-05454-4 Medline

14. Y. Fu, T. Wu, J. Wang, J. Zhai, M. J. Shearer, Y. Zhao, R. J. Hamers, E. Kan, K. Deng, X. Y. Zhu, S. Jin, Stabilization of the metastable lead iodide perovskite phase via surface functionalization. *Nano Lett.* **17**, 4405–4414 (2017). doi:10.1021/acs.nanolett.7b01500 Medline

15. S.-H. Turren-Cruz, A. Hagfeldt, M. Saliba, Methylammonium-free, high-performance, and stable perovskite solar cells on a planar architecture. *Science* **362**, 449–453 (2018). doi:10.1126/science.aat3583 Medline

16. M. Safdari, P. H. Svensson, M. T. Hoang, I. Oh, L. Kloo, J. M. Gardner, Layered 2D alkyldiammonium lead iodide perovskites: Synthesis, characterization, and use in solar cells. *J. Mater. Chem. A Mater. Energy Sustain.* **4**, 15638–15646 (2016). doi:10.1039/C6TA05055G

17. C. Ma, D. Shen, T.-W. Ng, M.-F. Lo, C.-S. Lee, C.-S. Lee, 2D perovskites with short interlayer distance for high-performance solar cell application. *Adv. Mater.* **30**, 1800710 (2018). doi:10.1002/adma.201800710

18. W.-Q. Wu, Z. Yang, P. N. Rudd, Y. Shao, X. Dai, H. Wei, J. Zhao, Y. Fang, Q. Wang, Y. Liu, Y. Deng, X. Xiao, Y. Feng, J. Huang, Bilateral alkylamine for suppressing charge recombination and improving stability in blade-coated perovskite solar cells. *Sci. Adv.* **5**, eaav8925 (2019). doi:10.1126/sciadv.aav8925 Medline

19. T. Zhao, C.-C. Chueh, Q. Chen, A. Rajagopal, A. K. Y. Jen, Defect passivation of organic–inorganic hybrid perovskites by diammonium iodide toward high-performance photovoltaic devices. *ACS Energy Lett.* **1**, 757–763 (2016). doi:10.1021/acsenergylett.6b00327

20. J. Lu, L. Jiang, W. Li, F. Li, N. K. Pai, A. D. Scully, C.-M. Tsai, U. Bach, A. N. Simonov, Y.-B. Cheng, L. Spiccia, Diammonium and monoammonium mixed-organic-cation perovskites for high performance solar cells with improved stability. *Adv. Energy Mater.* **7**, 1700444 (2017). doi:10.1002/aenm.201700444

21. X. Li, J. Hoffman, W. Ke, M. Chen, H. Tsai, W. Nie, A. D. Mohite, M. Kepenekian, C. Katan, J. Even, M. R. Wasielewski, C. C. Stoumpos, M. G. Kanatzidis, Two-Dimensional Halide Perovskites Incorporating Straight Chain Symmetric Diammonium Ions, $(NH_3C_mH_{2m}NH_3)(CH_3NH_3)_{n-1}Pb_nI_{3n+1}$ (m = 4-9; n = 1-4). *J. Am. Chem. Soc.* **140**, 12226–12238 (2018). doi:10.1021/jacs.8b07712 Medline

22. Y. Zhao, K. Zhu, CH3NH3Cl-assisted one-step solution growth of CH3NH3PbI3: Structure, charge-carrier dynamics, and photovoltaic properties of perovskite solar cells. *J. Phys. Chem. C* **118**, 9412–9418 (2014). doi:10.1021/jp502696w

23. F. Xie, C.-C. Chen, Y. Wu, X. Li, M. Cai, X. Liu, X. Yang, L. Han, Vertical recrystallization for highly efficient and stable formamidinium-based inverted-

structure perovskite solar cells. *Energy Environ. Sci.* **10**, 1942–1949 (2017). doi:10.1039/C7EE01675A

24. Y. Li, T. Zhang, F. Xu, Y. Wang, G. Li, Y. Yang, Y. Zhao, CH3NH3Cl assisted solvent engineering for highly crystallized and large grain size mixed-composition (FAPbI3)0.85(MAPbBr3)0.15 perovskites. *Crystals* **7**, 272 (2017). doi:10.3390/cryst7090272

25. A. Dubey, N. Adhikari, S. Mabrouk, F. Wu, K. Chen, S. Yang, Q. Qiao, Strategic review on processing routes towards highly efficient perovskite solar cells. *J. Mater. Chem. A Mater. Energy Sustain.* **6**, 2406–2431 (2018). doi:10.1039/C7TA08277K

26. M. Kim, G.-H. Kim, T. K. Lee, I. W. Choi, H. W. Choi, Y. Jo, Y. J. Yoon, J. W. Kim, J. Lee, D. Huh, H. Lee, S. K. Kwak, J. Y. Kim, D. S. Kim, Methylammonium chloride induces intermediate phase stabilization for efficient perovskite solar cells. *Joule* **3**, 2179–2192 (2019). doi:10.1016/j.joule.2019.06.014

27. Z. Wang, Y. Zhou, S. Pang, Z. Xiao, J. Zhang, W. Chai, H. Xu, Z. Liu, N. P. Padture, G. Cui, Additive-modulated evolution of HC(NH2)2PbI3 black polymorph for mesoscopic perovskite solar cells. *Chem. Mater.* **27**, 7149–7155 (2015). doi:10.1021/acs.chemmater.5b03169

28. C. Mu, J. Pan, S. Feng, Q. Li, D. Xu, Quantitative doping of chlorine in formamidinium lead trihalide (FAPbI3−xClx) for planar heterojunction perovskite solar cells. *Adv. Energy Mater.* **7**, 1601297 (2017). doi:10.1002/aenm.201601297

29. C. C. Stoumpos, C. D. Malliakas, M. G. Kanatzidis, Semiconducting tin and lead iodide perovskites with organic cations: Phase transitions, high mobilities, and near-infrared photoluminescent properties. *Inorg. Chem.* **52**, 9019–9038 (2013). doi:10.1021/ic401215x Medline

30. J.-W. Lee, D.-H. Kim, H.-S. Kim, S.-W. Seo, S. M. Cho, N.-G. Park, Formamidinium and cesium hybridization for photo- and moisture-stable perovskite solar cell. *Adv. Energy Mater.* **5**, 1501310 (2015). doi:10.1002/aenm.201501310

31. Z. Li, M. Yang, J.-S. Park, S.-H. Wei, J. J. Berry, K. Zhu, Stabilizing perovskite structures by tuning tolerance factor: formation of formamidinium and cesium lead iodide solid-state alloys. *Chem. Mater.* **28**, 284–292 (2016). doi:10.1021/acs.chemmater.5b04107

32. C. Yi, J. Luo, S. Meloni, A. Boziki, N. Ashari-Astani, C. Grätzel, S. M. Zakeeruddin, U. Röthlisberger, M. Grätzel, Entropic stabilization of mixed A-cation ABX3 metal halide perovskites for high performance perovskite solar cells. *Energy Environ. Sci.* **9**, 656–662 (2016). doi:10.1039/C5EE03255E

33. A. Binek, F. C. Hanusch, P. Docampo, T. Bein, Stabilization of the trigonal high-temperature phase of formamidinium lead iodide. *J. Phys. Chem. Lett.* **6**, 1249–1253 (2015). doi:10.1021/acs.jpclett.5b00380 Medline

34. A. D. Jodlowski, C. Roldán-Carmona, G. Grancini, M. Salado, M. Ralaiarisoa, S. Ahmad, N. Koch, L. Camacho, G. de Miguel, M. K. Nazeeruddin, Large guanidinium cation mixed with methylammonium in lead iodide perovskites for 19% efficient solar cells. *Nat. Energy* **2**, 972–979 (2017). doi:10.1038/s41560-017-0054-3

35. T. Yoon, G.-H. Kim, C. W. Myung, S. Kajal, J. Jeong, J. W. Kim, J. Y. Kim, K. S. Kim, Ambient-stable cubic-phase hybrid perovskite reaching the Shockley–Queisser fill

factor limit via inorganic additive-assisted process. *ACS Applied Energy Materials* **1**, 5865–5871 (2018). doi:10.1021/acsaem.8b01364

36. B. W. Park, N. Kedem, M. Kulbak, D. Y. Lee, W. S. Yang, N. J. Jeon, J. Seo, G. Kim, K. J. Kim, T. J. Shin, G. Hodes, D. Cahen, S. I. Seok, Understanding how excess lead iodide precursor improves halide perovskite solar cell performance. *Nat. Commun.* **9**, 3301 (2018). doi:10.1038/s41467-018-05583-w Medline

37. N. Liu, C. Yam, First-principles study of intrinsic defects in formamidinium lead triiodide perovskite solar cell absorbers. *Phys. Chem. Chem. Phys.* **20**, 6800–6804 (2018). doi:10.1039/C8CP00280K Medline

38. J. J. Yoo, S. Wieghold, M. C. Sponseller, M. R. Chua, S. N. Bertram, N. T. P. Hartono, J. S. Tresback, E. C. Hansen, J.-P. Correa-Baena, V. Bulović, T. Buonassisi, S. S. Shin, M. G. Bawendi, An interface stabilized perovskite solar cell with high stabilized efficiency and low voltage loss. *Energy Environ. Sci.* **12**, 2192–2199 (2019). doi:10.1039/C9EE00751B

39. Y. Liu, S. Akin, L. Pan, R. Uchida, N. Arora, J. V. Milić, A. Hinderhofer, F. Schreiber, A. R. Uhl, S. M. Zakeeruddin, A. Hagfeldt, M. I. Dar, M. Grätzel, Ultrahydrophobic 3D/2D fluoroarene bilayer-based water-resistant perovskite solar cells with efficiencies exceeding 22. *Sci. Adv.* **5**, eaaw2543 (2019). doi:10.1126/sciadv.aaw2543 Medline

40. H. Kim, S.-U. Lee, D. Lee, M. Paik, H. Na, J. Lee, S. I. Seok, Optimal interfacial engineering with different length of alkylammonium halide for efficient and stable perovskite solar cells. *Adv. Energy Mater.* (2019); https://doi.org/10.1002/aenm.201902740.

41. E. Mosconi, E. Ronca, F. De Angelis, First-principles investigation of the TiO2/organohalide perovskites interface: The role of interfacial chlorine. *J. Phys. Chem. Lett.* **5**, 2619–2625 (2014). doi:10.1021/jz501127k Medline

42. H. Tan, A. Jain, O. Voznyy, X. Lan, F. P. García de Arquer, J. Z. Fan, R. Quintero-Bermudez, M. Yuan, B. Zhang, Y. Zhao, F. Fan, P. Li, L. N. Quan, Y. Zhao, Z.-H. Lu, Z. Yang, S. Hoogland, E. H. Sargent, Efficient and stable solution-processed planar perovskite solar cells via contact passivation. *Science* **355**, 722–726 (2017). doi:10.1126/science.aai9081 Medline

43. F. X. Xie, D. Zhang, H. Su, X. Ren, K. S. Wong, M. Grätzel, W. C. H. Choy, Vacuum-assisted thermal annealing of CH3NH3PbI3 for highly stable and efficient perovskite solar cells. *ACS Nano* **9**, 639–646 (2015). doi:10.1021/nn505978r Medline

44. M. I. Saidaminov, J. Kim, A. Jain, R. Quintero-Bermudez, H. Tan, G. Long, F. Tan, A. Johnston, Y. Zhao, O. Voznyy, E. H. Sargent, Suppression of atomic vacancies via incorporation of isovalent small ions to increase the stability of halide perovskite solar cells in ambient air. *Nat. Energy* **3**, 648–654 (2018). doi:10.1038/s41560-018-0192-2

45. G. Kresse, J. Hafner, Ab initio molecular dynamics for liquid metals. *Phys. Rev. B Condens. Matter* **47**, 558–561 (1993). doi:10.1103/PhysRevB.47.558 Medline

46. G. Kresse, J. Hafner, Ab initio molecular-dynamics simulation of the liquid-metal-amorphous-semiconductor transition in germanium. *Phys. Rev. B Condens. Matter* **49**, 14251–14269 (1994). doi:10.1103/PhysRevB.49.14251 Medline

47. G. Kresse, J. Furthmüller, Efficiency of ab-initio total energy calculations for metals and semiconductors using a plane-wave basis set. *Comput. Mater. Sci.* **6**, 15–50 (1996). doi:10.1016/0927-0256(96)00008-0

48. G. Kresse, J. Furthmüller, Efficient iterative schemes for ab initio total-energy calculations using a plane-wave basis set. *Phys. Rev. B Condens. Matter* **54**, 11169–11186 (1996). doi:10.1103/PhysRevB.54.11169 Medline

49. P. E. Blöchl, Projector augmented-wave method. *Phys. Rev. B Condens. Matter* **50**, 17953–17979 (1994). doi:10.1103/PhysRevB.50.17953 Medline

50. J. P. Perdew, K. Burke, M. Ernzerhof, Generalized gradient approximation made simple. *Phys. Rev. Lett.* **77**, 3865–3868 (1996). doi:10.1103/PhysRevLett.77.3865 Medline